Columnar thin films for three-dimensional microbatteries

Fleischauer, M. D.; Li, Jing; Brett, M. J.

Publisher's version / Version de l'éditeur:
https://doi.org/10.1149/1.3006001
Journal of The Electrochemical Society, 156, 1, pp. A33-A36, 2008-11-05

Journal of The Electrochemical Society, **156** (1) A33-A36 (2009)
0013-4651/2008/156(1)/A33/4/$23.00 © The Electrochemical Society

Columnar Thin Films for Three-Dimensional Microbatteries

M. D. Fleischauer,[a,*,z] Jing Li,[b,] and M. J. Brett[a,c]**

[a]*National Research Council-National Institute for Nanotechnology, Edmonton, Alberta T6G 2M9, Canada*
[b]*Department of Chemistry, Dalhousie University, Halifax, Nova Scotia B3H 2J3, Canada*
[c]*Department of Electrical and Computer Engineering, University of Alberta, Edmonton, Alberta T6G 2V4, Canada*

Controlled-porosity Si thin films suitable for use as high-aspect-ratio microbattery electrodes were produced using the glancing angle deposition (GLAD) technique. GLAD is a high-vacuum physical vapor deposition method that can be used to produce a variety of film morphologies from most vacuum-compatible materials. No lithographic steps were required to create the porous, columnar thin films. Initial electrochemical results indicate large gravimetric and areal capacities (3600 mAh/g, 90 μAh/cm^2, respectively), and good capacity retention (3000 mAh/g after 70 charge/discharge cycles) can be obtained from Si vertical post morphology films. Areal capacity and capacity retention can likely be further improved by optimizing the film morphology, electrode material composition, and cycling conditions.
 [DOI: 10.1149/1.3006001]

Manuscript submitted April 28, 2008; revised manuscript received August 28, 2008. Published November 5, 2008.

Compact power sources are a critical component of modern electronics. Li-ion rechargeable batteries, common throughout portable electronics, typically occupy a significant volume fraction of the device they power. This can become an issue when device dimensions are on the millimeter or micrometer scale [e.g., microelectromechanical systems (MEMS)]. Thin-film Li-ion rechargeable batteries are able to provide energy densities similar to their full-size counterparts[1,2] but suffer from a common problem: because both full-size and thin film batteries are essentially planar in nature, a large electrode area is required to achieve significant capacity. Electrode thickness is limited by diffusion kinetics and other factors. Full-size battery electrodes are typically stacked, folded, or wrapped so that the overall cell is relatively compact. Thin-film batteries, in contrast, achieve large electrode areas by covering a large substrate area. Device power requirements therefore limit device miniaturization efforts. Many researchers are attempting to reduce the amount of substrate area (device "footprint") for a given capacity/volume of electrode material by moving from a planar two-dimensional (2D) to a three-dimensional (3D) electrode.[3] Here we demonstrate the fabrication of 3D columnar thin-film electrodes using the glancing angle deposition (GLAD) physical vapor deposition technique. This flexible and relatively simple process is well suited for microbattery development because column diameter, length, number density, and composition can be varied independently to fine-tune electrochemical performance.

There are relatively few ways to make 3D microbatteries. The challenge lies in creating two ordered interpenetrating electrodes separated by an electrolyte using MEMS-compatible techniques. Golodnitsky et al. are able to achieve significant capacity per unit substrate area gains by producing planar (2D) devices on a perforated (3D) substrate.[4] These gains can only be achieved after substantial processing, including etching through the Si substrate to create the perforations. Wang and Min et al. have fabricated aligned columns and full 3D microbatteries via photoresist pyrolysis,[5,6] which restricts the range of possible electrode materials. Other groups, focusing only on electrodes and not complete cells, have created aligned pores of various materials via etching Si,[7] vapor–(liquid)–solid growth of Si,[8] and numerous molding/templating methods (reviewed elsewhere).[3] 3D ordered macroporous electrodes/full cells have also demonstrated a great deal of potential,[9-11] although again, numerous processing steps are required.

Here we present a relatively simple, single-step high-vacuum technique that can be used to produce uniform aligned columns of most vacuum-compatible materials on almost any smooth substrate. GLAD has been used to fabricate controlled-porosity thin films with a variety of morphologies, including slanted posts, chevrons, square spirals, helices, vertical posts, and combinations thereof, on the tens to hundreds of nanometers scale.[12,13] A recent review of GLAD films and their applications is available elsewhere.[14] Morphology control, which depends on self-shadowing and limited adatom diffusion, is achieved via precise motion of the substrate relative to the incoming flux. A schematic of a typical GLAD apparatus is shown as Fig. 1. The angle between the incident vapor flux and the substrate normal, α, typically greater than 80°, has a large impact on overall film density/porosity and the spacing between individual features. Rotation about the substrate normal (rotation in ϕ) controls the chiral nature of the film (no rotation–slanted column, slow rotation–helix, fast rotation–vertical post). The purpose of this paper is to demonstrate that GLAD thin films, fabricated and characterized in less than ideal conditions, are suitable candidates for 3D microbattery electrodes.

Experimental

Controlled-porosity thin films were deposited onto as-provided stainless steel coin cell spacers (National Research Council - Institute for Chemical Process and Environmental Technology, Ottawa, ON, Canada) and Si(100) wafers using a modified Axxis high-vacuum electron beam evaporator (Kurt J. Lesker, Inc.). The system is cryopumped and regularly achieves base pressures in the low 10^{-8} Torr range. A 20 nm thick Cr (Cerac, 99.99%) adhesion layer

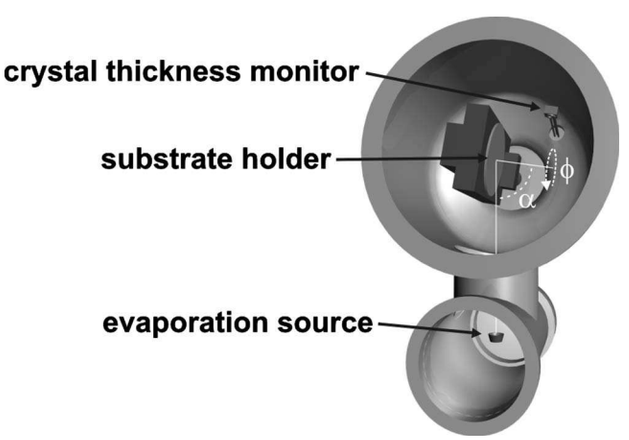

Figure 1. Schematic of the GLAD apparatus. Solid vertical and tilted white lines indicate the vapor flux direction and substrate normal, respectively. α and ϕ are described in the text.

* Electrochemical Society Active Member.
** Electrochemical Society Student Member.
z E-mail: mfleisch@ece.ualberta.ca

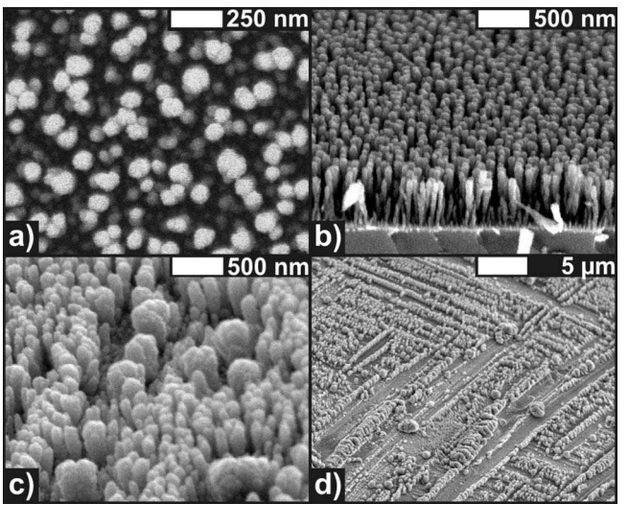

Figure 2. SEMs of 500 nm thick Si films deposited on a Si(100) wafer: (a) plan view, (b) oblique view, (c) an unpolished stainless steel disk, and (d) a 300 nm thick Si film on an unpolished stainless steel disk at lower magnification.

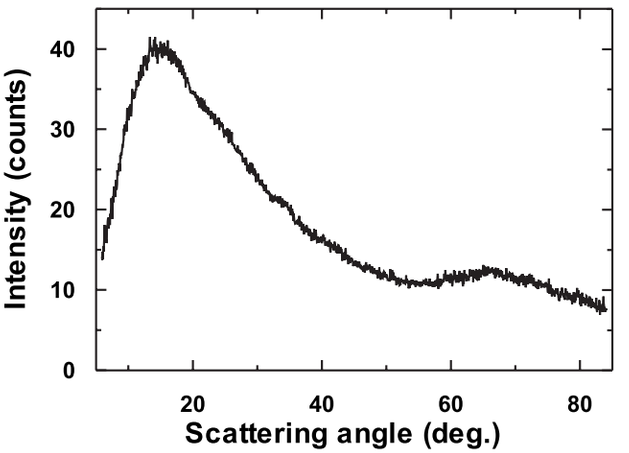

Figure 3. XRD pattern collected from a 500 nm thick Si film deposited on a Si(100) wafer.

was deposited at 10 Å/s at normal incidence, followed by the Si layer. Si (Kurt J. Lesker, Inc., 99.999%) was deposited at 10 Å/s with the flux incident 87° from the substrate normal. The substrate was rotated about its normal 50 times during the deposition of a 500 nm thick film. Film crystallinity was investigated using a Bruker D8 X-ray diffractometer equipped with a Cu target X-ray tube and an area detector. The beam incidence angle varied continuously from 3 to 40.5° during the collection of three separate frames at 20, 45, and 70° scattering angle.

Film mass was estimated by weighing 100 mm diam Si wafers before and after deposition of a nominally identical film using an A&D ER-182A balance and scaling to the area of the stainless steel spacers used during electrochemical testing. Si wafers were used for mass determination because they are flat over large areas, relatively lightweight, and of a known size.

Secondary electron scanning electron microscopy was performed prior to electrochemical testing using a JEOL 6301F field-emission scanning electron microscope (SEM). Electrochemical cycling was performed using 2325-type coin cell hardware and computer-controlled battery testers (E-One Moli Energy, Maple Ridge, BC, Canada). Coin cell assembly was performed in an Ar atmosphere glove box with less than 1 ppm O_2 and H_2O. The coin cell stack consisted of the can, a ~1.5 cm diam piece of Li foil, Celgard 2302 microporous polypropylene separator wet with six drops of electrolyte, the stainless steel spacer disk, a spring, and the cell top. A 1 M $LiPF_6$ sample in ethylene carbonate/diethyl carbonate (1:2 vol:vol) was used as the electrolyte.

Charge/discharge cycling was performed between either 5 or 170 mV and 1.2 V vs Li metal using the following routine. The first insertion was performed at 6 $\mu A/cm^2$. Subsequent cycling was performed in groups of 30 cycles: 10 cycles at 12 $\mu A/cm^2$, 10 cycles at 24 $\mu A/cm^2$, and 10 cycles at 48 $\mu A/cm^2$. These rates roughly correspond to C/8, C/4, and C/2, respectively, where n is the number of hours required to achieve the charge-storage capacity $C(C/n)$.

Results and Discussion

Self-shadowing is an important mechanism during GLAD. In order to obtain uniform films it is therefore critical that any initial self-shadowing be caused by adsorbed atoms or molecules, and not the substrate itself. The Si columns deposited on a Si(100) wafer shown in Fig. 2a and b are relatively uniform and evenly spaced, and resemble typical 3D microbattery electrode schematics. The average column diameter is approximately 100 nm. Because each column shadows its neighbors, small variations in column spacing lead to a distribution of column sizes. As the film thickness increases, individual columns grow, merge with nearby columns, or stop receiving flux. This competitive process takes place during the first few hundred nanometers of growth (as shown in Fig. 2b). Substrate seeding can be used to control feature spacing and produce a very narrow feature size distribution. A clear example of the effect of substrate seeding is available as Fig. 10 of Ref. 15. Additional nonlithographic techniques to improve feature uniformity are described elsewhere.[14] Column size distribution on seeded or unseeded substrates is uniform over a relatively large area (ca. 100 cm^2).

Si wafer roughness is typically on the order of a fraction of a nanometer, which means that even at high angles, most of the substrate is exposed to the flux. Stainless steel spacers were used for electrochemical testing. Although "new" spacers were used, numerous scratches visible to the naked eye were present prior to deposition. It is clear that the scratches shadow nearby areas and act as growth sites. No attempts to polish the disks were performed because of the unknown effects of polishing solutions and a lack of suitable equipment. We intend to investigate the effects of substrate roughness in the near future.

High- and low-magnification images of Si columns deposited on the steel spacers are shown as Fig. 2c and d, respectively. Some columns shown in Fig. 2c are similar in size to those shown in Fig. 2a and b (ca. 100 nm diam), but some are much larger (ca. 300 nm diam). The effect of the scratches is readily apparent in the lower magnification image shown in Fig. 2d. Unpolished stainless steel disks are far from ideal substrates but were used to simplify electrochemical testing.

The Si columns shown in Fig. 2 are smooth and without facets, suggesting the film is amorphous. An X-ray diffraction (XRD) pattern collected from a film deposited on a Si(100) wafer is provided as Fig. 3.[d] No sharp diffraction peaks are present, which confirms a lack of long-range ordering in the film. GLAD film crystallinity generally mirrors what would be expected from an evaporated or sputtered film of the same material (e.g., Ref. 14 and references within).

Differential capacity vs voltage curves for films cycled between 1.2 and 5 mV vs Li metal are shown in Fig. 4. Only curves from the 2nd, 32nd, and 62nd cycles (all at 12 $\mu A/cm^2$) are shown for the sake of clarity. These curves are quite similar to those collected from sputter-deposited amorphous Si,[16] and indicate Li is reacting only

[d] A very sharp peak at 69°, corresponding to the Si(400) diffraction peak, was not included in the integrated pattern.

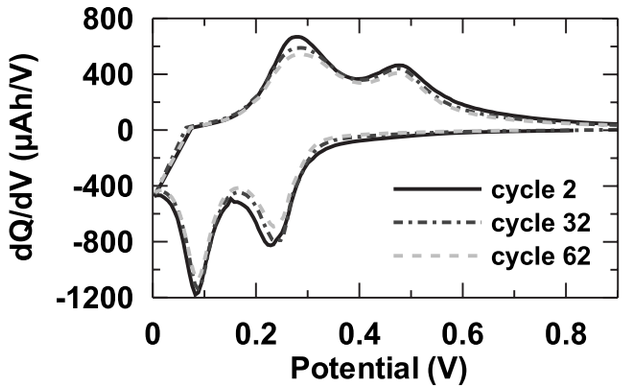

Figure 4. Differential capacity vs voltage curves from the 2nd, 32nd, and 62nd insertion/removal cycle (all at 12 $\mu A/cm^2$).

with Si to form amorphous Li_xSi. Origins of the slight capacity fade visible in Fig. 4 after 30 and 60 cycles are discussed shortly.

A full view of capacity vs cycle number is provided in Fig. 5. The average capacity fade was ~0.3%/cycle after 70 cycles. All capacities shown in Fig. 5 are presented in both mAh/g and $\mu Ah/cm^2$ to ease comparison with bulk and microbattery results. The first removal and subsequent insertion/removal capacities are within experimental uncertainty of the theoretical capacity of Si (3590 mAh/g at room temperature), which corresponds to the formation of $Li_{15}Si_4$ at full lithiation.[17] Uncertainty in gravimetric capacity values (±300 mAh/g) is almost entirely related to uncertainty in the film mass (60 ± 5 μg per stainless steel spacer). Similar gravimetric capacities have recently been demonstrated from ca. 100 nm diam Si fibers.[8] Chan et al. explained a first insertion capacity of 4200 mAh/g and 10 cycles at ~3500 mAh/g by assuming the presence of $Li_{4.4}Si$, no solid electrolyte interphase (SEI) formation, and ~20% irreversible capacity.[8] Our first insertion capacity of 5500 mAh/g is higher than that of all known Li–Si phases (4200 mAh/g, corresponding to $Li_{22}Si_5$, has been demonstrated at 415°C),[18] which implies some charge is consumed during SEI formation. Significant SEI formation should be expected when high-surface-area negative electrode materials are cycled using liquid electrolytes, as discussed in related Si and Ge nanowire work by Laik et al. and Chan et al.[19,20] Irreversible capacity, which can be associated with SEI formation if no other capacity loss mechanisms are present, was similar for nominally identical cells cycled to 5 mV and 0.17 V vs Li (105 and 70 μAh, respectively).

A plot of gravimetric capacity and coulombic efficiency as a function of cycle number for films cycled between 170 mV and

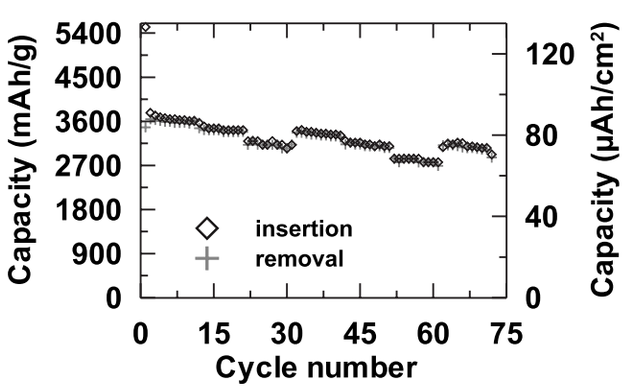

Figure 5. Capacity as a function of cycle number in mAh/g (left axis) and $\mu Ah/cm^2$ (right axis) for a cell cycled between 5 and 1.2 V.

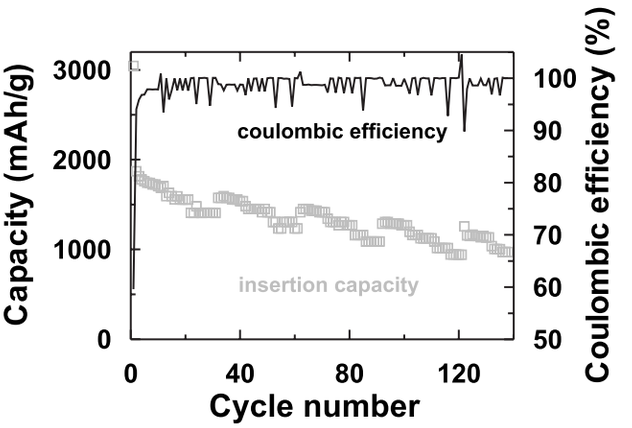

Figure 6. Capacity (mAh/g, left axis, gray squares) and coulombic efficiency (%, right axis, solid black line) as a function of cycle number for a cell cycled between 170 mV and 1.2 V.

1.2 V is provided as Fig. 6. The capacity fade was approximately 0.5% per cycle after 120 cycles. Scatter in the coulombic efficiency data is likely due to the charge/discharge rate changing every 10 cycles and limitations of the cycling equipment. We are currently developing a high-precision, low-current charge/discharge system to address these limitations in future work.

Film mass on the steel spacer was confirmed to be equivalent to that on a Si wafer within experimental uncertainty (±10 μg), as determined by weighing before and after deposition. This is not surprising as the flux incident per unit substrate area depends only on deposition parameters (e.g., deposition rate, angle of incidence) and not the substrate itself. No evidence for differing sticking coefficients between steel and Si wafers was observed. Cycling was performed in three groups of 10 cycles at 12, 24, and 48 $\mu A/cm^2$ in order to explore the rate capability of these high-surface-area electrodes. Good capacity retention can be observed (after the initial insertion) at all three rates, and most capacity loss associated with higher-rate cycling can be returned by cycling at lower rates. A 500 nm thick film of solid Si should have a capacity of 420 $\mu Ah/cm^2$ (and very bad rate capability) based on a volumetric capacity of 8365 mAh/cm^3 for Si. It is clear from Fig. 2, especially Fig. 2a, that the films are far from solid and are approximately 3/4 porous. Capacity and mass measurements suggest a film porosity of 80%, which is somewhat higher than other reported values (71%).[21] We fabricated a highly porous film because electrolyte and a second electrode (likely of lower volumetric capacity) must be incorporated within the structure of a complete 3D microbattery.

Coulombic efficiencies were typically 99% after the first five cycles. Although 99% coulombic efficiency is too low for commercial cells, these results already compare favorably with existing porous/nanowire negative electrode literature,[8,19,22] and further improvements should be possible. These aligned Si posts, which have an aspect ratio of ~5, were able to undergo more than 70 dramatic volume changes (ca. 300%)[23] without breaking or separating from the electrode. Li alloying with Si at room temperature forms crystalline $Li_{15}Si_4$ below 50 mV vs Li metal,[17] which can lead to two-phase regions and significant capacity fade. Hatchard and Dahn later proposed that the formation of crystalline $Li_{15}Si_4$ is suppressed in solid films thinner than ~2 μm.[24] This may be related to work of Graetz et al.,[25] who suggested that crack propagation could not occur for Si particles ~300 nm or less in size. If each post is considered a particle, then the post diameter is far smaller than Graetz's critical dimension, but the height is not. An increase in film thickness, and therefore capacity, would likely lead to similar capacity retention behavior. Capacities of up to ca. 500 $\mu Ah/cm^2$ (with similar capacity retention and rate capability) can be envisioned from a

2.5 μm thick film. Additional capacity could also be obtained by decreasing the film porosity and increasing the average post diameter by depositing films at lower flux incidence angles (e.g., $\alpha = 80–85°$).

The results presented here represent a two to threefold capacity increase over a solid Si film with similar rate capability (i.e., a film as thick as the average post radius, ca. 50 nm). These results were obtained with coin cells and a liquid electrolyte, which is vastly different than most views of commercialized 3D microbatteries. Deposition on a smooth surface would improve post uniformity and likely improve capacity retention appreciably, because some of the capacity fade may be the result of some of the larger posts, especially like those shown in Fig. 2d, cracking and separating from the electrode. Further capacity retention improvements can probably be achieved by incorporating a solid or polymeric electrolyte within the aligned pores. Film composition, morphology, and density/porosity can also be independently adjusted to fine-tune electrode performance.

Conclusions

Controlled-porosity Si thin films consisting of high-aspect-ratio vertical posts can undergo more than 70 insertion/removal cycles without significant capacity fade. The 500 nm thick, ca. 80% porous thin film had a reversible capacity of over 90 $\mu Ah/cm^2$, more than twice what could be expected from a solid film with similar rate capability (i.e., approximately half the post diameter, or ca. 50 nm thick). Higher areal capacities can likely be realized by simply increasing the film thickness. Because good capacity retention was obtained from a material known to undergo large volume changes, even better capacity retention can be expected from most other common thin-film electrode materials.

Acknowledgments

This work was supported by the Natural Sciences and Engineering Research Council of Canada (NSERC), the Informatics Circle of Research Excellence (iCORE), and Micralyne, Incorporated. M.F. acknowledges NSERC, Alberta Ingenuity, and the Killam Trusts for fellowship support. The authors thank Professor C. Lucy for the use of his balance.

National Researach Council-National Institute for Nanotechnology assisted in meeting the publication costs of this article.

References

1. S. D. Jones and J. R. Akridge, *Solid State Ionics*, **69**, 357 (1994).
2. J. B. Bates, N. J. Dudney, B. Neudecker, A. Ueda, and C. D. Evans, *Solid State Ionics*, **135**, 33 (2000).
3. J. W. Long, B. Dunn, D. R. Rolison, and H. S. White, *Chem. Rev. (Washington, D.C.)*, **104**, 4463 (2004).
4. D. Golodnitsky, M. Nathan, V. Yufit, E. Strauss, K. Freedman, L. Burstein, A. Gladkich, and E. Peled, *Solid State Ionics*, **177**, 2811 (2006).
5. C. Wang, L. Taherabadi, G. Jia, M. Madou, Y. Yeh, and B. Dunn, *Electrochem. Solid-State Lett.*, **7**, A435 (2004).
6. H.-S. Min, B. Y. Park, L. Taherabadi, C. Wang, Y. Yeh, R. Zaouk, M. J. Madou, and B. Dunn, *J. Power Sources*, **178**, 795 (2008).
7. M. Green, E. Fielder, B. Scrosati, M. Wachtler, and J. S. Moreno, *Electrochem. Solid-State Lett.*, **6**, A75 (2003).
8. C. K. Chan, H. Peng, G. Liu, K. McIlwrath, X. F. Zhang, R. A. Huggins, and Y. Cui, *Nat. Nanotechnol.*, **3**, 31 (2008).
9. J. S. Sakamoto and B. Dunn, *J. Mater. Chem.*, **12**, 2859 (2002).
10. K. Dokko, N. Akutagawa, Y. Isshiki, K. Hoshina, and K. Kanamura, *Solid State Ionics*, **176**, 2345 (2005).
11. N. S. Ergang, J. C. Lytle, K. T. Lee, S. M. Oh, W. H. Smyrl, and A. Stein, *Adv. Mater. (Weinheim, Ger.)*, **18**, 1750 (2006).
12. K. Robbie and M. J. Brett, *J. Vac. Sci. Technol. A*, **15**, 1460 (1997).
13. K. J. Robbie and M. J. Brett, U.S. Pat. 5,866,204.
14. J. J. Steele and M. J. Brett, *J. Mater. Sci.: Mater. Electron.*, **18**, 367 (2007).
15. M. O. Jensen and M. J. Brett, *IEEE Trans. Nanotechnol.*, **4**, 269 (2005).
16. M. D. Fleischauer, R. Mar, and J. R. Dahn, *J. Electrochem. Soc.*, **154**, A151 (2007).
17. M. N. Obrovac and L. Christensen, *Electrochem. Solid-State Lett.*, **7**, A93 (2004).
18. C. J. Wen and R. A. Huggins, *J. Solid State Chem.*, **37**, 271 (1981).
19. B. Laik, L. Eude, J. P. Pereria-Ramos, C. S. Cojocaru, D. Pribat, and E. Rouviére, *Electrochim. Acta*, **17**, 5528 (2008).
20. C. K. Chan, X. F. Zhang, and Y. Cui, *Nano Lett.*, **8**, 307 (2008).
21. K. Kaminska, A. Amassian, L. Martinu, and K. Robbie, *J. Appl. Phys.*, **97**, 013511 (2005).
22. R. Figueroa, T. G. S. Cruz, and A. Gorenstein, *J. Power Sources*, **172**, 422 (2007).
23. L. Y. Beaulieu, K. W. Eberman, R. L. Turner, L. J. Krause, and J. R. Dahn, *Electrochem. Solid-State Lett.*, **4**, A137 (2001).
24. T. D. Hatchard and J. R. Dahn, *J. Electrochem. Soc.*, **151**, A838 (2004).
25. J. Graetz, C. C. Ahn, R. Yazami, and B. Fultz, *Electrochem. Solid-State Lett.*, **6**, A194 (2003).